IJMMM International Journal of Minerals, Metallurgy and Materials 矿物冶金与材料学报（英文版）

Assessing the corrosion protection property of coatings loaded with corrosion inhibitors using the real-time atmospheric corrosion monitoring technique

Xiaoxue Wang, Lulu Jin, Jinke Wang, Rongqiao Wang, Xiuchun Liu, Kai Gao, Jingli Sun, Yong Yuan, Lingwei Ma, Hongchang Qian, and Dawei Zhang

Cite this article as:
Xiaoxue Wang, Lulu Jin, Jinke Wang, Rongqiao Wang, Xiuchun Liu, Kai Gao, Jingli Sun, Yong Yuan, Lingwei Ma, Hongchang Qian, and Dawei Zhang, Assessing the corrosion protection property of coatings loaded with corrosion inhibitors using the real-time atmospheric corrosion monitoring technique, *Int. J. Miner. Metall. Mater.*, 32(2025), No. 1, pp. 119-126. https://doi.org/10.1007/s12613-024-2860-5

View the article online at SpringerLink or IJMMM Webpage.

Articles you may be interested in

Nikhil, Gopal Ji, and Rajiv Prakash, Hydrothermal synthesis of Zn–Mg-based layered double hydroxide coatings for the corrosion protection of copper in chloride and hydroxide media, *Int. J. Miner. Metall. Mater.*, 28(2021), No. 12, pp. 1991-2000. https://doi.org/10.1007/s12613-020-2122-0

Navid Mehdipour, Milad Rezaei, and Zeynab Mahidashti, Influence of glycine additive on corrosion and wear performance of electroplated trivalent chromium coating, *Int. J. Miner. Metall. Mater.*, 27(2020), No. 4, pp. 544-554. https://doi.org/10.1007/s12613-020-1975-6

Chun-duo Dai, Yu Fu, Jia-xiang Guo, and Cui-wei Du, Effects of substrate temperature and deposition time on the morphology and corrosion resistance of $FeCoCrNiMo_{0.3}$ high-entropy alloy coating fabricated by magnetron sputtering, *Int. J. Miner. Metall. Mater.*, 27(2020), No. 10, pp. 1388-1397. https://doi.org/10.1007/s12613-020-2149-2

Muhammad Ahsan Iqbal and Michele Fedel, Ordering and disordering of *in situ* grown MgAl-layered double hydroxide and its effect on the structural and corrosion resistance properties, *Int. J. Miner. Metall. Mater.*, 26(2019), No. 12, pp. 1570-1577. https://doi.org/10.1007/s12613-019-1844-3

Wei-ning Shi, Shu-feng Yang, and Jing-she Li, Effect of nonmetallic inclusions on localized corrosion of spring steel, *Int. J. Miner. Metall. Mater.*, 28(2021), No. 3, pp. 390-397. https://doi.org/10.1007/s12613-020-2018-z

Jing Ma, Fan Feng, Bai-qing Yu, Hai-feng Chen, and Li-feng Fan, Effect of cooling temperature on the microstructure and corrosion behavior of X80 pipeline steel, *Int. J. Miner. Metall. Mater.*, 27(2020), No. 3, pp. 347-353. https://doi.org/10.1007/s12613-019-1882-x

IJMMM WeChat

QQ author group

INTERNATIONAL JOURNAL OF
Minerals, Metallurgy and Materials

Volume 32, Number 1, January 2025
Page 119

Research Article https://doi.org/10.1007/s12613-024-2860-5

Assessing the corrosion protection property of coatings loaded with corrosion inhibitors using the real-time atmospheric corrosion monitoring technique

Xiaoxue Wang[1,2], *Lulu Jin*[3], *Jinke Wang*[3], *Rongqiao Wang*[1], *Xiuchun Liu*[2], *Kai Gao*[2], *Jingli Sun*[5], *Yong Yuan*[5], *Lingwei Ma*[3,4]✉, *Hongchang Qian*[3]✉, *and Dawei Zhang*[3,4]✉

1) School of Energy and Power Engineering, Beihang University, Beijing 100191, China
2) Beijing Institute of Space Long March Vehicle, Beijing 100076, China
3) National Materials Corrosion and Protection Data Center, University of Science and Technology Beijing, Beijing 100083, China
4) Institute of Materials Intelligent Technology, Liaoning Academy of Materials, Shenyang 110004, China
5) Shanghai Spaceflight Precision Machinery Institute, Shanghai 201600, China
(Received: 16 December 2023; revised: 8 February 2024; accepted: 22 February 2024)

Abstract: The atmospheric corrosion monitoring (ACM) technique has been widely employed to track the real-time corrosion behavior of metal materials. However, limited studies have applied ACM to the corrosion protection properties of organic coatings. This study compared a bare epoxy coating with one containing zinc phosphate corrosion inhibitors, both applied on ACM sensors, to observe their corrosion protection properties over time. Coatings with artificial damage via scratches were exposed to immersion and alternating dry and wet environments, which allowed for monitoring galvanic corrosion currents in real-time. Throughout the corrosion tests, the ACM currents of the zinc phosphate/epoxy coating were considerably lower than those of the blank epoxy coating. The trend in ACM current variations closely matched the results obtained from regular electrochemical tests and surface analysis. This alignment highlights the potential of the ACM technique in evaluating the corrosion protection capabilities of organic coatings. Compared with the blank epoxy coating, the zinc phosphate/epoxy coating showed much-decreased ACM current values that confirmed the effective inhibition of zinc phosphate against steel corrosion beneath the damaged coating.

Keywords: atmospheric corrosion monitoring technology; corrosion inhibitor; coating; carbon steel; corrosion protection

1. Introduction

Organic coatings are among the most efficient and practical approaches for protecting metal materials [1–2]. However, their barrier function faces numerous external threats, such as complex aging conditions, corrosive media, or mechanical harm [3–5]. Once these external factors destroy the organic coating matrix, a corrosive medium will rapidly penetrate through coating defects, reaching the underlying metal substrate and sparking corrosion. Persistent corrosion on a metal substrate drastically shortens its lifespan, potentially leading to safety hazards [6–7]. To fortify the corrosion protection of organic coatings, an effective strategy is to add corrosion inhibitors into the coating matrix [8–10]. These inhibitors form a protective layer on the metal surface, shielding it from direct contact with a corrosive medium, thus endowing the coatings with passive protective properties. Furthermore, in the event of coating damage, the inhibitor layer formed at the defects effectively curbs the corrosion process. Consequently, the integration of corrosion inhibitors into anti-corrosion coatings has been a focus of the field of corrosion and protection for decades [11–14].

Although corrosion-resistant coatings incorporating inhibitors have been extensively designed and studied, assessing their anti-corrosion properties largely relies on traditional *ex-situ* methods, such as electrochemical characterization [15–17] or surface composition analysis [18–20]. Although these methods evaluate the corrosion protection status or failure behavior of organic coatings at specific times, they cannot monitor real-time variations in their corrosion protection performance [21].

Recently, the atmospheric corrosion monitoring (ACM) technique has garnered considerable interest for instantaneously monitoring the corrosion resistance of metal materials [22–24]. ACM captures transient corrosion activities through an instantaneous galvanic current [25–26], the impedance modulus [27–28], or electrochemical noise values [29]. For example, Mizuno *et al*. [30] installed Fe/Ag double-electrode ACM sensors on vehicles for a three-month atmospheric exposure corrosion test. By comparing galvanic current integral values from ACM sensors with the corrosion rate of steel coupons, they found a strong linear correlation

✉ Corresponding authors: Lingwei Ma E-mail: mlw1215@ustb.edu.cn; Hongchang Qian E-mail: qianhc@ustb.edu.cn; Dawei Zhang E-mail: dzhang@ustb.edu.cn

Springer

with a coefficient of 0.913. Furthermore, Pei *et al*. [31] combined the ACM technique with machine learning to investigate the correlation between the corrosion rate and various environmental factors, highlighting the substantial impact of rust formation on the corrosion prediction model.

Given the success of ACM in monitoring metal material corrosion, we propose using this technique to promptly detect the corrosion protection status of organic coatings. To test our hypothesis, we applied epoxy coatings with and without zinc phosphate corrosion inhibitors onto ACM sensor surfaces. Artificial scratches were introduced onto the coatings to simulate external mechanical damage. These sensors with different scratched coatings were exposed to immersion and alternating dry/wet environments to track the variation in corrosion protection properties. The morphology and elemental composition of the steel electrode surface beneath the scratches were analyzed using scanning electron microscopy (SEM) and energy dispersive spectroscopy (EDS). Moreover, electrochemical impedance spectroscopy (EIS) was applied to the various scratched coatings after specific immersion times to characterize their corrosion protection properties, aiming to confirm the reliability of ACM technology in monitoring the corrosion protection of organic coatings.

2. Experimental

2.1. Materials

Bisphenol A diglycidyl ether (DGEBA), Jeffamine D230 curing agent, and zinc phosphate hydrate were procured from Aladdin Chemical Co., Ltd. Ethanol, acetone, and sodium chloride (NaCl) were supplied by Sinopharm Chemical Reagent. All chemicals and solvents were used in their original form. To construct galvanic corrosion couples, Q235 carbon steel and graphite sheets served as the anodes and cathodes, respectively. The chemical composition of the carbon steel is found in Table 1.

Table 1. Chemical composition of Q235 carbon steel wt%

C	Mn	Si	S	Fe
0.15	0.50	0.30	0.05	In balance

2.2. Preparation of ACM sensors

A schematic of the ACM sensor, depicted in Fig. 1, comprises seven sets of steel/graphite galvanic couples. Glass fiber-reinforced epoxy composite boards, 0.1 mm thick, provide electrical insulation between the carbon steel and galvanic electrodes. Each carbon steel anode of the galvanic electrode pair exposes an area of 21 mm × 1 mm. When an electrolyte film forms on the sensor surface, the steel and graphite electrodes link, initiating a galvanic corrosion current. Lead wires connect the ACM sensors to the micro-galvanometer and data logger, which monitor and record the current [31].

2.3. Preparation of the zinc phosphate/epoxy coatings

The ACM sensors underwent sequential abrasion using 150-, 240-, and 400-grit sandpapers before use, followed by ultrasonic cleaning with acetone and ethanol. The epoxy resin, comprising DAGBA and Jeffamine D230 at a molar ratio of 2:1, was prepared [32]. Initially, 15wt% zinc phosphate, relative to the weight of the epoxy coating matrix, was dispersed into DGEBA at 50°C under stirring for 3 h. This mixture was then combined with Jeffamine D230, stirred for an additional 15 min, and spread over the ACM sensor surface using a rod applicator. The applied coating, named ZP-15%, was cured at 55°C for 24 h [33].

Moreover, a reference specimen, the blank epoxy coating

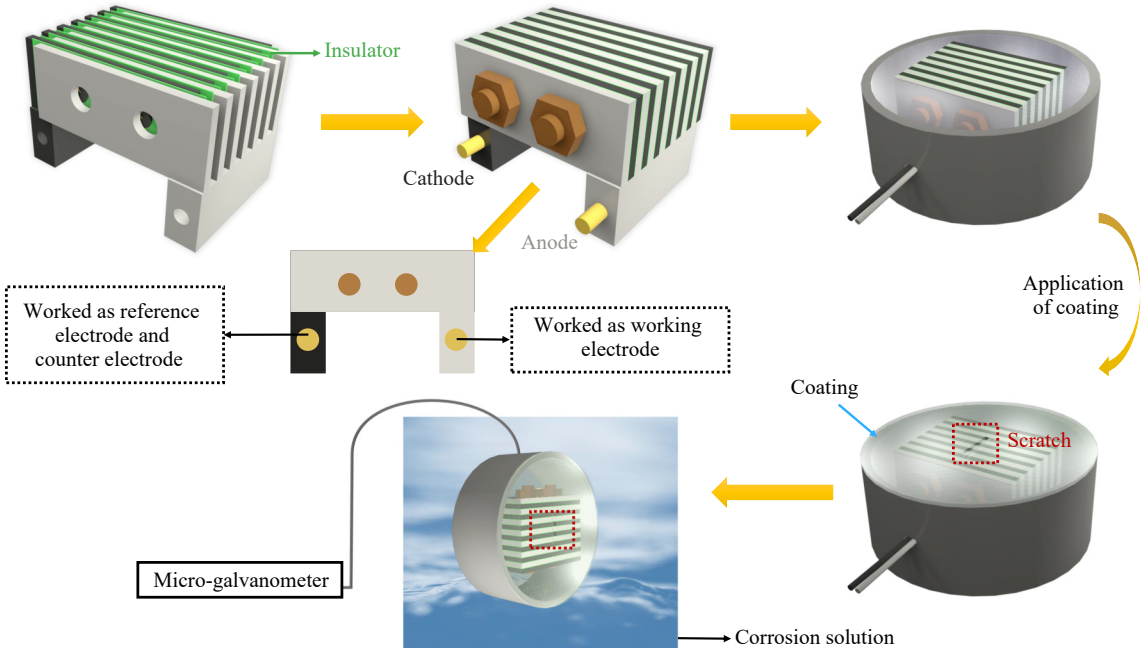

Fig. 1. Schematic of the coated steel/graphite ACM sensor.

without any additive, was prepared and termed ZP-0% coating. The dry coating thickness of all specimens was measured at (60 ± 10) μm.

2.4. Characterization of coatings

Initially, an artificial scratch was made approximately 80 μm wide and 5 mm long across three pairs of steel/graphite electrode couples on the ZP-0% and ZP-15% coatings. Subsequently, the ACM sensors with these different coatings were exposed to immersion and alternating dry/wet environments to investigate the corrosion protection variations. The alternating dry/wet experiments were conducted in a home-designed EA-08 type alternating dry/wet corrosion test chamber. For both environments, the electrolyte was a 3.5wt% NaCl solution. Each dry/wet cycle comprised 60 min, with 40 min of drying (at 40°C and (60 ± 5)% humidity) followed by 20 min of immersion in the electrolyte (at 25°C) [34]. The main experiments were conducted following GB/T 19746-2018. These coated ACM sensors were subjected to an alternating dry/wet environment for 9 d. Micro-galvanometers monitored and recorded corrosion currents in real-time, reflecting the corrosion behavior at the scratched areas of the coating, with current values being logged every minute.

Additionally, EIS measurements were conducted using an electrochemical workstation (PARSTAT 2273, AMETEK) to further explore the corrosion resistance of the different scratched coatings. The carbon steel electrode of the ACM sensor served as the working electrode, while the graphite electrode was used as the auxiliary and reference electrodes [35–36]. EIS measurements encompassed a frequency range of 10^5 to 10^{-2} Hz with a sinusoidal voltage perturbation of 20 mV. The surface morphologies of different coatings were observed using SEM (Regulus SU8100) equipped with EDS.

3. Results and discussion

3.1. Real-time corrosion monitoring in a NaCl immersion environment

Fig. 2(a) depicts the instantaneous variation in the galvanic current ($I_{ACM\text{-}instant}$) of ACM sensors with different scratched coatings over a 7-d immersion period. Initially, during the immersion phase, the corrosion medium swiftly penetrated the sensor probe surface through the artificial scratch, initiating a galvanic current between the carbon steel anode and the graphite cathode. Consequently, the ZP-0% and ZP-15% coatings exhibited $I_{ACM\text{-}instant}$ values of approximately 30 nA. As immersion time elapsed, the scratched ZP-0% coating demonstrated a gradual increase in $I_{ACM\text{-}instant}$, reaching approximately 70 nA after 80 h of immersion, signifying escalated corrosion activity at the scratched area. Conversely, the $I_{ACM\text{-}instant}$ of the scratched ZP-15% coating decreased to approximately 20 nA within 12 h because a zinc phosphate inhibition layer rapidly formed at the scratched coating area. Throughout the prolonged immersion, the $I_{ACM\text{-}instant}$ of the scratched ZP-15% coating consistently remained at ~20 nA,

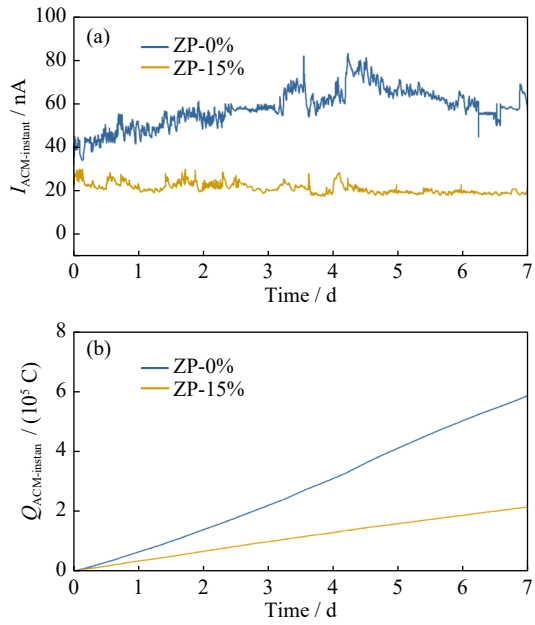

Fig. 2. Variation in current of ACM sensor $I_{ACM\text{-}instant}$ (a) and electric quantity of ACM sensor $Q_{ACM\text{-}instant}$ (b) of ACM sensors coated with different scratched coatings over 7 d of immersion in 3.5wt% NaCl solution.

indicating sustained long-term inhibition performance.

To further quantify the corrosion extent of the carbon steel electrode at the scratched areas of different coatings, the $I_{ACM\text{-}instant}$ values were integrated over the immersion period, generating the electrical quantity output of the ACM sensors ($Q_{ACM\text{-}instant}$) using Eq. (1) for a data acquisition interval of 1 min [37].

$$Q_{ACM-instant} = \sum_{n=1}^{n=T} (I_1 + I_2 + I_3 + \cdots + I_n)\,\Delta t \quad (1)$$

where I_n is the $I_{ACM\text{-}instant}$ value at the moment $n = t$ (t = 1, 2, 3, …, T), and Δt is the time data acquisition interval, which is 1 min in this study.

As depicted in Fig. 2(b), $Q_{ACM\text{-}instant}$ has a lower slope for the scratched ZP-15% coating than for the scratched ZP-0% coating, suggesting a lower corrosion degree for the carbon steel anode coated with ZP-15%. The $Q_{ACM\text{-}instant}$ value of the scratched ZP-0% coating was approximately three times higher than that of the ZP-15% coating, primarily due to the corrosion inhibition effect induced by zinc phosphate.

3.2. Corrosion inhibition mechanism of the ZP-15% coating

EIS measurements were performed to further validate the corrosion inhibition property of zinc phosphate within the scratched areas of the coatings. As illustrated in Fig. 3, the capacitive reactance arcs of the ZP-0% coating were always smaller than those of the ZP-15% coating during 7 d of immersion in 3.5wt% NaCl solution, indicating the better corrosion protection property of the coating with zinc phosphate corrosion inhibitors. Typically, the low-frequency impedance modulus at 0.01 Hz ($|Z|_{0.01Hz}$) indicates the corrosion protection efficacy of coatings [38–39]. During immersion, the $|Z|_{0.01Hz}$ values for the scratched ZP-0% coating gradually

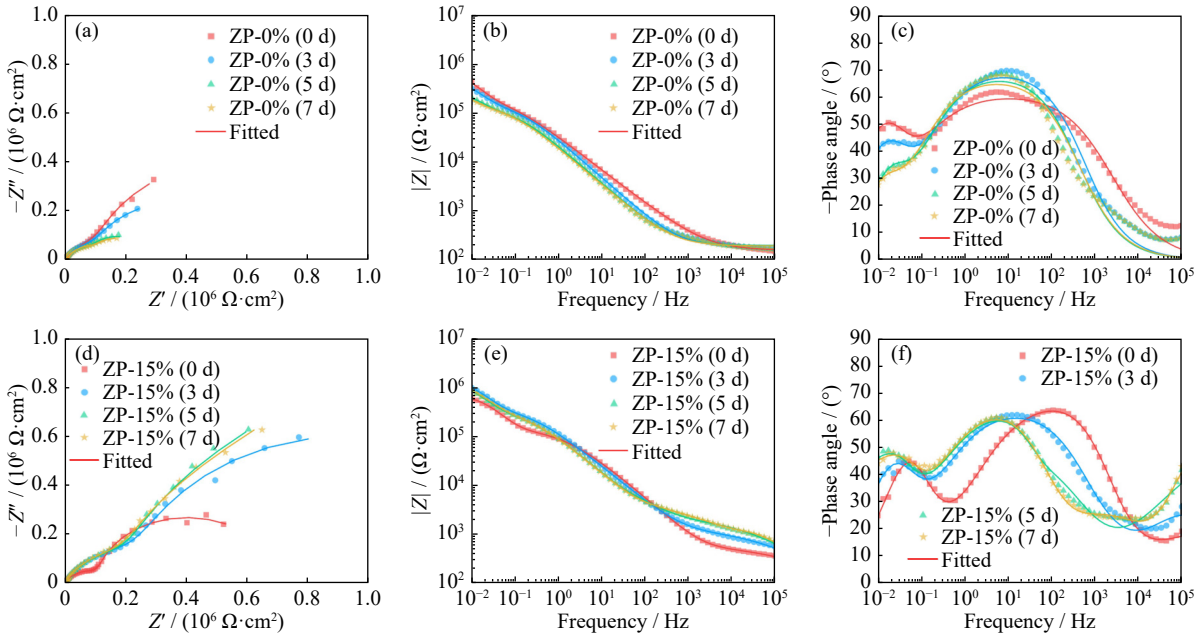

Fig. 3. Nyquist diagram and Bode–impedance modulus plots of (a–c) the ZP-0% coating and (d–f) the ZP-15% coating during 7 d of immersion in 3.5wt% NaCl solution.

decreased because of the escalating corrosion reaction. Conversely, the $|Z|_{0.01Hz}$ values for the scratched ZP-15% coating progressively increased to approximately 10^6 Ω·cm^2 after 3 d of immersion and remained consistent during subsequent immersion periods. Even after 7 d of immersion, the $|Z|_{0.01Hz}$ value for the scratched ZP-15% coating was nearly one order of magnitude higher than that of the scratched ZP-0% coating, showcasing the robust corrosion protection capability of the ZP-15% coating. From the phase angle plots, the phase angle values at high frequencies reflect the barrier property of coatings. The ZP-15% coating exhibited higher phase angles at 10^5 Hz, indicating its better corrosion protection property [40–42].

Figs. 4(a) and (b) showcase the SEM images capturing the carbon steel surface beneath the scratches of ZP-0% and ZP-15% coatings, respectively. Substantial loose corrosion products are evident in the image for the ZP-0% coating, contrasting with the noticeably reduced and more densely packed corrosion products beneath the scratch of the ZP-15% coating. In addition, Fig. 4(c) illustrates the elemental composition of the corrosion products at the scratch of ZP-15% coating, indicating the presence of Zn and P. These EDS result demonstrates that zinc phosphate effectively suppressed corrosion product accumulation and prevented coating-failure [43–44].

Upon comparing the real-time monitoring outcomes of ACM sensors with the results from electrochemical analysis and corrosion morphology examination, a similar trend in the corrosion degrees in the scratched areas is observed using both methods. This comparison indicates the viability of the ACM technique for assessing the corrosion protection efficacy and failure behavior of organic coatings. In the subsequent section, the ACM sensors with various scratched coatings were subjected to an alternating dry/wet environment to further evaluate the corrosion protection performance of epoxy coatings integrated with zinc phosphate.

3.3. Real-time corrosion monitoring in an alternating dry/wet environment

Fig. 5 illustrates the $I_{ACM\text{-}instant}$ of ACM sensors with scratched ZP-0% coatings during alternating dry/wet tests. In Fig. 5(a), the $I_{ACM\text{-}instant}$ variation for the scratched ZP-0%

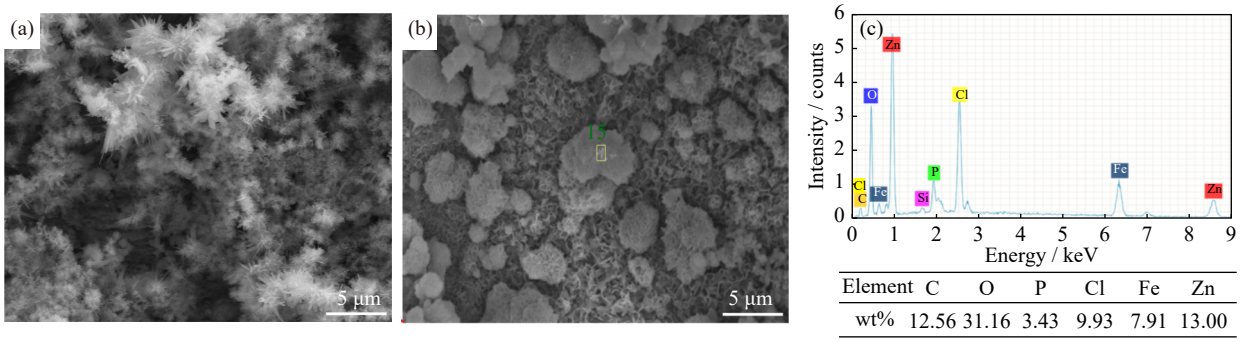

Element	C	O	P	Cl	Fe	Zn
wt%	12.56	31.16	3.43	9.93	7.91	13.00

Fig. 4. SEM images of the steel surface underneath the scratches of (a) ZP-0% coating and (b) ZP-15% coating. (c) EDS result of steel underneath the scratched area of ZP-15% coating after 7 d of immersion in 3.5wt% NaCl solution.

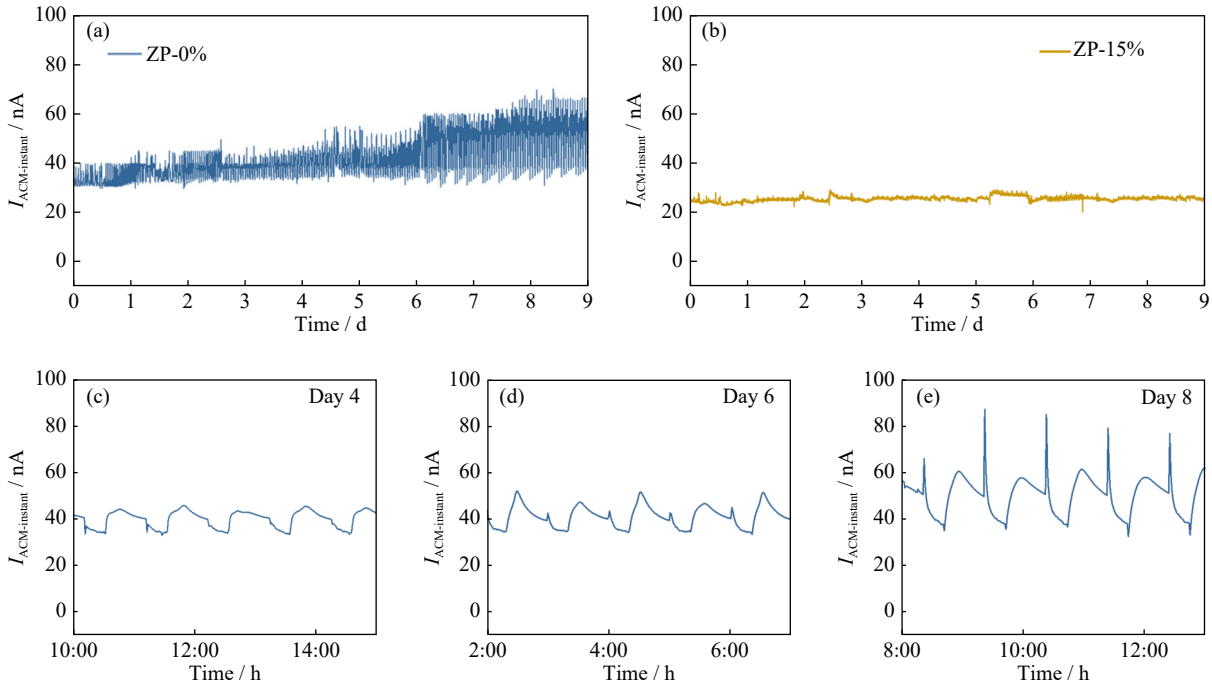

Fig. 5. $I_{ACM\text{-}instant}$ **of ACM sensors coated with the scratched ZP-0% (a) and ZP-15% (b) coatings throughout the alternating dry/wet test.** $I_{ACM\text{-}instant}$ **on different specific durations for ZP-0% coating: (c) from 10:00 AM to 3:00 PM on Day 4; (d) from 2:00 AM to 7:00 AM on Day 6; (e) from 8:00 AM to 1:00 PM on Day 8.**

coating exhibits periodic behavior with a gradually increasing amplitude. This periodicity corresponds to the cycles of alternating wet and dry environments. Further delineated in Fig. 5(c)–(e) is the $I_{ACM\text{-}instant}$ variations for the scratched ZP-0% coating at specific intervals. The amplitude of $I_{ACM\text{-}instant}$ variation increases from approximately 10 nA on Day 4 to more than 40 nA on Day 8, indicating an escalation of corrosion activity.

In contrast, the $I_{ACM\text{-}instant}$ of the scratched ZP-15% coating displays minimal evident cyclical fluctuations, consistently remaining at ~25 nA throughout the alternating dry/wet test (seen in Fig. 5(b)). This stability can be attributed to the early formation of a relatively steadfast corrosion inhibitor film by zinc phosphate on the scratch of the coating during the initial phase of the alternating dry/wet test. Despite the cyclic shift in environmental conditions from wet to dry, the infiltration of the corrosive medium was effectively suppressed, preventing further deterioration of the corrosion process.

To determine the variation in $I_{ACM\text{-}instant}$ of ACM sensors coated with different coatings in the alternating dry/wet environment, the change rate of $I_{ACM\text{-}instant}$ was calculated by differentiation, termed as $I'_{ACM\text{-}instant}$. As depicted in Fig. 6(a), the $I'_{ACM\text{-}instant}$ values of the scratched ZP-0% coating sharply fluctuated around zero throughout the alternating dry/wet test. This volatility arises primarily from the unprotected exposed steel surface at the scratch of the ZP-0% coating, causing abrupt changes in corrosion activity with the shift between wet and dry environments. In contrast, the $I'_{ACM\text{-}instant}$ values of the scratched ZP-15% coating consistently approached zero, indicating a relatively stable $I_{ACM\text{-}instant}$ value during the alternating dry/wet test, attributed to the inhibition effect of zinc phosphate.

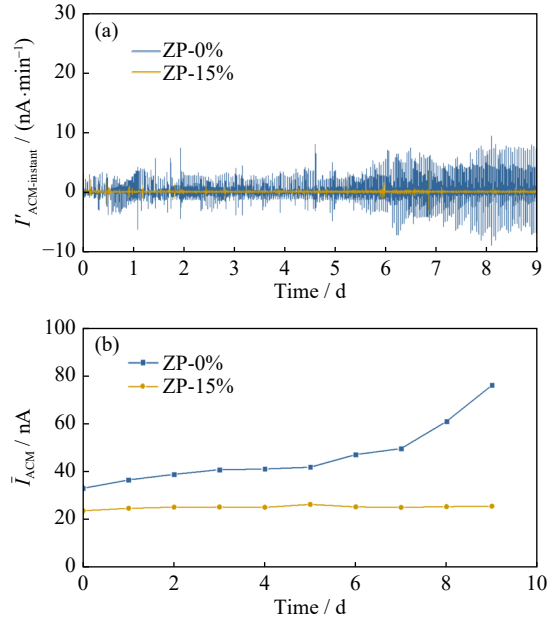

Fig. 6. $I'_{ACM\text{-}instant}$ **(a) and** $\bar{I}_{ACM}$ **(b) of ACM sensors coated with the scratched ZP-15% coating throughout the alternating dry/wet test.**

To eliminate the influence of periodic changes in the $I_{ACM\text{-}instant}$ value, the daily average value of $I_{ACM\text{-}instant}$ (denoted as $\bar{I}_{ACM}$) was calculated to analyze the trend in the variation in galvanic corrosion current values for different scratched coatings [45]. As depicted in Fig. 6(b), over 9 d of testing, $\bar{I}_{ACM}$ increased from ~33 to ~77 nA for the scratched ZP-0% coating and slowly increased from ~23 to ~25 nA for the scratched ZP-15% coating.

Furthermore, the corrosion progression of ACM sensors

coated with various scratched coatings during the alternating dry/wet test was assessed through the variation in $Q_{ACM\text{-}instant}$, as illustrated in Fig. 7. Notably, the slope of $Q_{ACM\text{-}instant}$ for the scratched ZP-15% coating was observed to be considerably lower than that of the scratched ZP-0% coating, similar to the results observed in the immersion environment. This comparison suggests that zinc phosphate provides ample corrosion inhibition even in alternating dry and wet environments for damaged coatings.

Fig. 8 displays the morphology of ACM sensors coated with different scratched coatings during the alternating dry/wet test. Following a day of testing, some corrosion rust was visible at the scratches of ZP-0% and ZP-15% coatings. With increasing test duration, rust formation increased substantially, notably more pronounced and expansive in the case of the scratched ZP-0% coating. The accumulation of corrosion products delaminated the coating scratch and severely corroded the metal electrode [46–47]. Conversely, fewer corrosion products were observed on the ZP-15% coating, further substantiating the corrosion protection attributes conferred by zinc phosphate to the steel substrate.

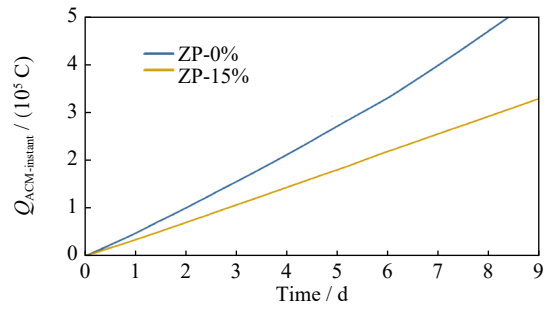

Fig. 7. $Q_{ACM\text{-}instant}$ variation in ACM sensors coated with different scratched coatings throughout the alternating dry/wet test.

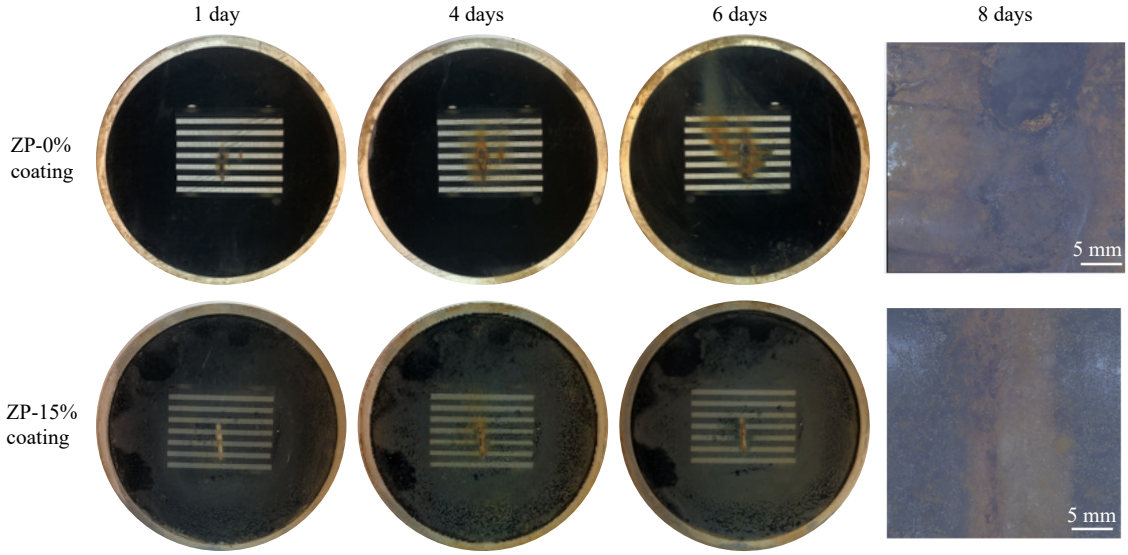

Fig. 8. Optical pictures of the ACM sensors coated with different scratched coatings throughout the alternating dry/wet test.

4. Conclusion

In summary, a steel/graphite ACM sensor was used to monitor the instantaneous variation in the galvanic current of a steel electrode beneath a coating scratch, assessing the corrosion protection efficacy of zinc phosphate/epoxy coatings. Throughout the immersion, the ACM current consistently remained substantially lower for the scratched ZP-15% coating than for the scratched ZP-0% coating. EIS measurements highlighted that the scratched ZP-15% coating surpassed the scratched ZP-0% coating in the $|Z|_{0.01Hz}$ value by nearly one order of magnitude after 7 d of immersion. Furthermore, the steel electrode surface beneath the scratch of the ZP-15% coating displayed fewer corrosion products, reaffirming the corrosion inhibition potential of zinc phosphate. During the alternating dry/wet test, the scratched ZP-15% coating exhibited notably lower and more stable ACM values than the scratched ZP-0% coating, confirming the superior corrosion protection performance of the ZP-15% coating. Consequently, the ACM technique demonstrates considerable promise in evaluating the corrosion protection attributes of organic coatings in real-time.

Acknowledgements

This work was financially supported by the National Natural Science Foundation of China (No. 52371049), the Young Elite Scientists Sponsorship Program by the China Association for Science and Technology (YESS, No. 2020QNRC001), and the National Science and Technology Resources Investigation Program of China (Nos. 2021FY100603 and 2019FY101404).

Conflicts of Interest

Dawei Zhang is an editorial board member for this journal and was not involved in the editorial review or the decision to publish this article. The authors declare no conflict of interest.

References

[1] F. Zhang, P.F. Ju, M.Q. Pan, *et al*., Self-healing mechanisms in smart protective coatings: A review, *Corros. Sci.*, 144(2018), p. 74.

[2] D. Wang, C. Ma, J.Y. Liu, *et al*., Corrosion resistance and anti-soiling performance of micro-arc oxidation/graphene oxide/stearic acid superhydrophobic composite coating on magnesium alloys, *Int. J. Miner. Metall. Mater.*, 30(2023), No. 6, p. 1128.

[3] C. Ma, D. Wang, J.Y. Liu, N. Peng, W. Shang, and Y.Q. Wen, Preparation and property of self-sealed plasma electrolytic oxide coating on magnesium alloy, *Int. J. Miner. Metall. Mater.*, 30(2023), No. 5, p. 959.

[4] M. Cheng, Q. Fu, B. Tan, *et al*., Build a bridge from polymeric structure design to engineering application of self-healing coatings: A review, *Prog. Org. Coat.*, 167(2022), art. No. 106790.

[5] J.K. Wang, W.M. Tan, H. Yang, *et al*., Towards weathering and corrosion resistant, self-warning and self-healing epoxy coatings with tannic acid loaded nanocontainers, *npj Mater. Degrad.*, 7(2023), art. No. 39.

[6] B.R. Hou, X.G. Li, X.M. Ma, *et al*., The cost of corrosion in China, *npj Mater. Degrad.*, 1(2017), art. No. 4.

[7] X.G. Li, D.W. Zhang, Z.Y. Liu, Z. Li, C.W. Du, and C.F. Dong, Materials science: Share corrosion data, *Nature*, 527(2015), No. 7579, p. 441.

[8] L. Zhao, J.K. Wang, K. Chen, *et al*., Functionalized carbon dots for corrosion protection: Recent advances and future perspectives, *Int. J. Miner. Metall. Mater.*, 30(2023), No. 11, p. 2112.

[9] Y.J. Wang, J.K. Wang, L.W. Ma, *et al*., Qualitative and quantitative detection of corrosion inhibitors using surface-enhanced Raman scattering coupled with multivariate analysis, *Appl. Surf. Sci.*, 568(2021), art. No. 150967.

[10] Y.N. Wang, C.F. Dong, D.W. Zhang, P.P. Ren, L. Li, and X.G. Li, Preparation and characterization of a chitosan-based low-pH-sensitive intelligent corrosion inhibitor, *Int. J. Miner. Metall. Mater.*, 22(2015), No. 9, p. 998.

[11] T. Yimyai, D. Crespy, and M. Rohwerder, Corrosion-responsive self-healing coatings, *Adv. Mater.*, 35(2023), No. 47, art. No. e2300101.

[12] L. Wang, S.N. Li, and J.J. Fu, Self-healing anti-corrosion coatings based on micron-nano containers with different structural morphologies, *Prog. Org. Coat.*, 175(2023), art. No. 107381.

[13] Y. Huang, P.J. Wang, W.M. Tan, *et al*., Photothermal and pH dual-responsive self-healing coating for smart corrosion protection, *J. Mater. Sci. Technol.*, 107(2022), p. 34.

[14] X.Y. Wang, S. Liu, J. Yan, J.P. Zhang, Q.Y. Zhang, and Y. Yan, Recent progress of polymeric corrosion inhibitor: Structure and application, *Materials*, 16(2023), No. 8, art. No. 2954.

[15] J.M. He, W.X. Xu, H. Liu, *et al*., Preparation of a novel 2-amino benzothiazole loaded ZIF-8/layer double hydroxide composite and its application in anti-corrosion epoxy coatings, *Prog. Org. Coat.*, 185(2023), art. No. 107927.

[16] J.K. Wang, L.W. Ma, Z.B. Chen, *et al*., Multi-channel preparation and high-throughput screening of coating fillers with optimized corrosion sensing and inhibition properties for smart protective coatings, *Corros. Sci.*, 222(2023), art. No. 111390.

[17] L. Cheng, C.B. Liu, H. Wu, H.C. Zhao, and L.P. Wang, A two-dimensional nanocontainer based on mesoporous polydopamine coated lamellar hydroxyapatite towards anticorrosion reinforcement of waterborne epoxy coatings, *Corros. Sci.*, 193(2021), art. No. 109891.

[18] J.J. Zhao, A. Santoso, and S.J. Garcia, Small concentrations of NaCl help building stable inhibiting layers from 2, 5-dimercapto-1, 3, 4-thiadiazole (DMTD) on AA2024-T3, *Corros. Sci.*, 225(2023), art. No. 111562.

[19] H. Khosravi, R. Naderi, and B. Ramezanzadeh, Designing an epoxy composite coating having dual-barrier-active self-healing anti-corrosion functions using a multi-functional GO/PDA/MO nano-hybrid, *Mater. Today Chem.*, 27(2023), art. No. 101282.

[20] X. Liu, Z.Y. Gao, D. Wang, F.J. Yu, B.S. Du, and I. Gitsov, Improving the protection performance of waterborne coatings with a corrosion inhibitor encapsulated in polyaniline-modified halloysite nanotubes, *Coatings*, 13(2023), No. 10, art. No. 1677.

[21] K. Bijapur, V. Molahalli, A. Shetty, A. Toghan, P. De Padova, and G. Hegde, Recent trends and progress in corrosion inhibitors and electrochemical evaluation, *Appl. Sci.*, 13(2023), No. 18, art. No. 10107.

[22] D. Xu, Z.B. Pei, X.J. Yang, *et al*., A review of trends in corrosion-resistant structural steels research-from theoretical simulation to data-driven directions, *Materials*, 16(2023), No. 9, art. No. 3396.

[23] D.H. Xia, C.M. Deng, D. Macdonald, *et al*., Electrochemical measurements used for assessment of corrosion and protection of metallic materials in the field: A critical review, *J. Mater. Sci. Technol.*, 112(2022), p. 151.

[24] J.H. Ahn, Y.S. Jeong, I.T. Kim, S.H. Jeon, and C.H. Park, A method for estimating time-dependent corrosion depth of carbon and weathering steel using an atmospheric corrosion monitor sensor, *Sensors*, 19(2019), No. 6, art. No. 1416.

[25] X.J. Yang, Y. Yang, M.H. Sun, *et al*., A new understanding of the effect of Cr on the corrosion resistance evolution of weathering steel based on big data technology, *J. Mater. Sci. Technol.*, 104(2022), p. 67.

[26] Q. Li, X.J. Xia, Z.B. Pei, *et al*., Long-term corrosion monitoring of carbon steels and environmental correlation analysis via the random forest method, *npj Mater. Degrad.*, 6(2022), art. No. 1.

[27] A. Nishikata, Q.J. Zhu, and E. Tada, Long-term monitoring of atmospheric corrosion at weathering steel bridges by an electrochemical impedance method, *Corros. Sci.*, 87(2014), p. 80.

[28] S. Wan, J. Hou, Z.F. Zhang, X.X. Zhang, and Z.H. Dong, Monitoring of atmospheric corrosion and dewing process by interlacing copper electrode sensor, *Corros. Sci.*, 150(2019), p. 246.

[29] D.H. Xia, S.Z. Song, W.X. Jin, *et al*., Atmospheric corrosion monitoring of field-exposed Q235B and T91 steels in Zhoushan offshore environment using electrochemical probes, *J. Wuhan Univ. Technol. Mater. Sci. Ed.*, 32(2017), No. 6, p. 1433.

[30] D. Mizuno, S. Suzuki, S. Fujita, and N. Hara, Corrosion monitoring and materials selection for automotive environments by using atmospheric corrosion monitor (ACM) sensor, *Corros. Sci.*, 83(2014), p. 217.

[31] Z.B. Pei, D.W. Zhang, Y.J. Zhi, *et al*., Towards understanding and prediction of atmospheric corrosion of an Fe/Cu corrosion sensor via machine learning, *Corros. Sci.*, 170(2020), art. No. 108697.

[32] T. Xie and I.A. Rousseau, Facile tailoring of thermal transition temperatures of epoxy shape memory polymers, *Polymer*, 50(2009), No. 8, p. 1852.

[33] K. Gong, M. Wu, and G.X. Liu, Comparative study on corrosion behaviour of rusted X100 steel in dry/wet cycle and immersion environments, *Constr. Build. Mater.*, 235(2020), art. No. 117440.

[34] J.K. Wang, L.W. Ma, Y. Huang, *et al*., Photothermally activated self-healing protective coating based on the “close and seal” dual-action mechanisms, *Composites Part B*, 231(2022), art. No. 109574.

[35] C. Qiao, Q. Wu, L. Hao, *et al*., Material selection in making electrochemical impedance spectroscopy sensor for electrolyte thickness measurement in marine atmosphere, *Corros. Sci.*, 221(2023), art. No. 111373.

[36] Z.W. Zou, G.L. Song, Z.M. Wang, and D.J. Zheng, A novel single-electrode AC probe for rapid monitoring of both instant-

aneous and accumulated electrochemical parameters in corrosion, *Electrochim. Acta*, 321(2019), art. No. 134664.
[37] Z.B. Pei, X.Q. Cheng, X.J. Yang, *et al*., Understanding environmental impacts on initial atmospheric corrosion based on corrosion monitoring sensors, *J. Mater. Sci. Technol.*, 64(2021), p. 214.
[38] B.F. Fan, J.J. Yang, L. Cao, *et al*., Revealing the impact of micro-SiO_2 filer content on the anti-corrosion performance of water-borne epoxy resin, *Polymers*, 15(2023), No. 15, art. No. 3273.
[39] L.W. Ma, J.K. Wang, Y.J. Wang, *et al*., Enhanced active corrosion protection coatings for aluminum alloys with two corrosion inhibitors co-incorporated in nanocontainers, *Corros. Sci.*, 208(2022), art. No. 110663.
[40] R. Raj, Y. Morozov, L.M. Calado, *et al*., Inhibitor loaded calcium carbonate microparticles for corrosion protection of epoxy-coated carbon steel, *Electrochim. Acta*, 319(2019), p. 801.
[41] M. Mahdavian and M.M. Attar, Another approach in analysis of paint coatings with EIS measurement: Phase angle at high frequencies, *Corros. Sci.*, 48(2006), No. 12, p. 4152.
[42] L.W. Ma, J.K. Wang, D.W. Zhang, *et al*., Dual-action self-healing protective coatings with photothermal responsive corrosion inhibitor nanocontainers, *Chem. Eng. J.*, 404(2021), art. No. 127118.
[43] Y.T. Wu, S.G. Wen, K.M. Chen, J.H. Wang, G.Y. Wang, and K. Sun, Enhanced corrosion resistance of waterborne polyurethane containing sulfonated graphene/zinc phosphate composites, *Prog. Org. Coat.*, 132(2019), p. 409.
[44] H.X. Wan, D.D. Song, X.G. Li, D.W. Zhang, J. Gao, and C.W. Du, Effect of zinc phosphate on the corrosion behavior of water-borne acrylic coating/metal interface, *Materials*, 10(2017), No. 6, art. No. 654.
[45] Z.B. Pei, K. Xiao, L.H. Chen, *et al*., Investigation of corrosion behaviors on an Fe/Cu-type ACM sensor under various environments, *Metals*, 10(2020), No. 7, art. No. 905.
[46] D.D. Song, H.X. Wan, X.H. Tu, and W. Li, A better understanding of failure process of waterborne coating/metal interface evaluated by electrochemical impedance spectroscopy, *Prog. Org. Coat.*, 142(2020), art. No. 105558.
[47] N. Wint, C.M. Griffiths, C.J. Richards, G. Williams, and H.N. McMurray, The role of benzotriazole modified zinc phosphate in preventing corrosion-driven organic coating disbondment on galvanised steel, *Corros. Sci.*, 174(2020), art. No. 108839.